NASA TM X-1391

EXPERIMENTAL EVALUATION OF HIGH-PURITY-SILICA REINFORCED ABLATIVE COMPOSITES AS NOZZLE SECTIONS OF 7.8-INCH-(19.8 CM) DIAMETER THROAT STORABLE-PROPELLANT ROCKET ENGINE

By Donald A. Peterson

Lewis Research Center
Cleveland, Ohio

NATIONAL AERONAUTICS AND SPACE ADMINISTRATION

For sale by the Clearinghouse for Federal Scientific and Technical Information
Springfield, Virginia 22151 – CFSTI price $3.00

EXPERIMENTAL EVALUATION OF HIGH-PURITY-SILICA REINFORCED ABLATIVE COMPOSITES AS NOZZLE SECTIONS OF 7.8-INCH-(19.8 CM) DIAMETER THROAT STORABLE-PROPELLANT ROCKET ENGINE

by Donald A. Peterson

Lewis Research Center

SUMMARY

Eleven high-purity-silica reinforced ablative materials were evaluated as nozzle sections of a storable propellant (nitrogen tetroxide and a blend of 50-percent unsymmetrical dimethylhydrazine and 50-percent hydrazine) rocket engine. Testing was performed at an oxidant-to-fuel ratio of 2.0, a chamber pressure of 100 psia (689 kN/m^2) and an initial throat diameter of 7.82 inches (19.8 cm). Both oxidant-to-fuel ratio and chamber pressure were maintained constant during the test firing at an equivalent pressure altitude of 1.60 psia (11.05 kN/m^2).

Erosion rates, char information, and a discussion of the effect on erosion of some major material and processing variables are presented.

INTRODUCTION

Reinforced plastics are being used extensively for ablative cooling applications in both liquid and solid rocket-engine thrust chambers. System design simplicity together with versatility of fabrication of chambers are definite advantages contributing to overall reliability. However, the primary problem requiring attention is excessive throat erosion or sacrificial mass loss which is responsible for engine-performance losses during the operating life of the thrust chamber. Since the specific-impulse losses are inversely proportional to engine-throat size at a constant erosion rate, the engine-performance losses are most severe in small engines. As engines increase in size, structural requirements also increase; thus, in addition to a high erosion resistance, a large ablative engine should also possess high char strength at low char rates to minimize weight requirements.

Prior to a study of optimization of ablative composites, a class of ablative materials must be chosen which will exhibit reasonable ablative characteristics in a given combustion environment. Generally, for any given class of ablative materials, the radial erosion rate is primarily a function of the surface temperature and the oxidation or reduction potential in the boundary layer. Two recently completed investigations were conducted to evaluate several types of commercially available ablative materials as nozzle sections of a hydrogen-oxygen rocket engine (ref. 1) and of a storable-propellant (nitrogen tetroxide N_2O_4 and a 50-50 blend of unsymmetrical dimethylhydrazine UDMH with hydrazine N_2H_4) engine (ref. 2). The ablative materials in both investigations were tested at a nominal chamber pressure and throat diameter of 100 psia (689 kN/m^2) and 1.20 inches (3.04 cm), respectively. Similar results were obtained with respect to the relative order of throat-erosion resistance for the various material classes. The high-purity-silica reinforced materials had, as a class, erosion resistance superior to all material classes tested.

The primary objective of the present investigation was to evaluate the erosion resistance of several high-purity-silica reinforced ablative materials as nozzle sections of a 7.8-inch-(19.8 cm) diameter throat (nominal Apollo sizes), storable-propellant rocket engine. A secondary objective was to perform a preliminary study of the effects on erosion of some major material and processing variables including resin content and cloth-fiber diameter. The nominal engine conditions included an oxidant-to-fuel ratio of 2.00, constant chamber pressure of 100 psia (689 kN/m^2), and an initial throat diameter of 7.82 inches (19.8 cm). All testing was conducted at an ambient pressure of 1.60 psia (11.05 kN/m^2). Results are presented for 11 high-purity-silica reinforced ablative materials in terms of nozzle-throat dimensional change as a function of run time. Char thickness, if it is available, is presented as percent char, from original thickness, to the outer asbestos insulation.

APPARATUS

Ablative-Material Samples

No attempt was made to correlate results with a particular material supplier as samples were chosen for their basic constituents only without regard to the source.

The ablative-material samples evaluated in the present investigation are listed in table I. The samples have been numbered in the order presented in the table, and this number is used herein to identify the samples. In addition, the table lists all pertinent information which is necessary to adequately describe each sample. Four nozzles with the cloth layed up in a rosette, six nozzles with fibers oriented 90° to the centerline, and one nozzle with material of 1/2-inch chopped squares (1.27-cm squares) were tested. A

rosette-type fiber orientation is layed up in plies which run longitudinally, at a given helix angle, in contrast to fabric layed up circumferentially with respect to the nozzle centerline. Figure 1 shows nozzles with a typical rosette layup, a standard fiber-orientation angle of 90^{o}, and chopped material of 1/2-inch squares. Two of the 90^{o} fiber-orientation nozzles (6 and 7) were hand impregnated by the supplier after removal of all the fill fibers. All the remaining fibers were radially oriented with respect to the nozzle centerline. The phenolic resin used in all samples conformed to the requirements of specification MIL-R-9299. Sample 3 was intended to be a direct comparison with sample 2 to assess the effect of a modified chromium salt additive to an 0.008-inch (0.203 mm) and a 0.015 inch (0.381 mm) fiber diameter, respectively. However, the chromium salts in the smaller fiber-diameter material were difficult to convert into the modified form, and, therefore, a proprietary resin was used as a substitute in an attempt to duplicate this modification during the firing. The rosette nozzles were layed up in a female tool and hydroclaved at 1000-psia (6894 kN/m^2) pressure, and the remaining nozzles were compression molded in matched metal dies at 3000-psia (20 660 kN/m^2) pressure.

Facility

The experimental test runs were conducted in the altitude facility shown in figure 2. A view of the test chamber area is shown in figure 3. A test engine mounted to the thrust stand and the entrance to the exhaust collector can be seen.

The fuel (50-50 blend of UDMH and hydrazine) tank had a capacity of 560 gallons (2.12 m^3) while the oxidant (N_2O_4) tank capacity is 707 gallons (2.67 m^3). A capability for over 400 seconds continuous operation was therefore possible at a chamber pressure of 100 psia (689 kN/m^2), an oxidant-to-fuel ratio of 2.0, and a constant throat diameter of 7.82 inches (19.8 cm).

Rotating equipment exhausted the test chamber to 1.60 psia (11.05 kN/m^2). Combustion products were funnelled through the water-cooled exhaust collector and finally discharged approximately 60 feet (18.23 m) above ground level into the atmosphere.

Engine

The basic engine common to all tests consisted of an injector as shown in the photographs of figures 4 and 5 and a water-cooled combustion chamber detailed in figure 6. A typical ablative nozzle is shown in figure 7.

The injector used for the entire program consisted of 127 triplet elements arranged

in a circular pattern. Elements were drilled on a slightly convergent angle directed toward the chamber centerline (fig. 5) and radially oriented to provide impinging fans nominally parallel to the chamber wall. All elements had two fuel streams of 0.043-inch (1.09 mm) diameter, each impinging on one oxidant stream of 0.0785-inch (2.0 mm) diameter at an included angle of 20° and a distance of 0.56 inch (14.23 mm). The nominal oxidant and fuel-injection differential pressures were 40 (275 kN/m^2) and 50 psia (344 kN/m^2), respectively. AA 6061-T6 aluminum was used throughout. A water-flow test is shown in figure 5.

The water-cooled cylindrical combustion chamber was used in conjunction with the ablative-nozzle section for all testing. The chamber (copper) had an inside diameter of 10.77 inches (27.3 cm) and was 18.0 inches (45.7 cm) long. A 0.005-inch (1.27 mm) coating of nickel was applied to the inside diameter to increase corrosion resistance. Water-inlet pressure of 200 psia (1378 kN/m^2) provided 350 gallons (1.325 m^3) per minute water-flow rate for cooling. Two identical chambers were used alternately throughout the program.

The ablative nozzle (fig. 7) consisted of a steel housing with attachment flange (not show) which was bolted to the water-cooled chamber. An epoxy sealant was used to bond the ablative specimen into the housing and to provide a hot-gas seal at the chamber nozzle interface.

The basic engine assembly was 23.0 inches (58.5 cm) long, from injector to nozzle throat, and had a characteristic chamber length L* of 43.0 with contraction and expansion ratios of 1.90 and 1.85, respectively. The nozzle-entrance half angle was 30° which converged to a 7.82-inch (19.8 cm) throat and expanded at a half angle of 15°. All test firings were performed in a horizontal test stand.

Instrumentation

The combustion-chamber pressure was taken from two taps drilled into the injector face and measured by strain-gage-type pressure transducers. Flow rates for each propellant were measured by both venturi and turbine-type flow meters. Thrust was measured by a double-bridge strain-gage load cell. Thermocouples were installed in both propellant lines and injector domes.

Recording and Processing

All electric outputs were digitalized, sampled at a rate of 4000 samples per second, and recorded on magnetic tape. Selected outputs were also recorded by multichannel

oscillograph and strip-chart recording instruments for control-room data reduction and system monitoring. The data on magnetic tape were first checked on an oscilloscope display unit and then fed into a computer along with the appropriate calibration and conversion constants for processing.

PROCEDURE

Testing

The operation of the instrumentation was verified, and the engine assembly pressure checked prior to each run. The propellant tanks were loaded and pressurized with nitrogen gas. The closed-loop controller was set to maintain a constant chamber pressure of 100 psia (689 kN/m^2) and an oxidant-to-fuel ratio of 2.0 during the firing duration. Changes in chamber pressure due to throat area change were compensated by corresponding changes in the propellant-flow rate. The altitude chamber was evacuated to approximately 1.60-psia (11.05 kN/m^2) pressure, and the high-pressure pumps were activated to supply cooling water to the chamber. A sequence timer automatically activated appropriate valves, data acquisition equipment, and propellant-line purges for each run. An oscilloscope was used to monitor possible combustion instability (determined from a water-cooled flush-mount pressure transducer located on the inside diameter of the combustion chamber). An abort switch was normally activated 1 to 2 seconds after detection of any high-frequency instability (usually 2200 cycles per second (2200 Hz), 1st tangential mode). On these few occasions, the restarted engine was free of high-frequency instability.

All ablative nozzles were subjected to a single continuous firing duration of at least 250 seconds. Nozzles 4, 5, 7, 8, and 10 were arbitrarily run for longer continuous durations to check on gouging potential and to determine if the steady-state erosion rate was appreciably changed when char to the insulation was evident. The throat diameter of each ablative nozzles was measured before and after running, and each was subsequently sectioned for visual inspection and photographed. Char-thickness measurements were obtained for nine of the nozzles tested.

Calculations

The combustion-performance level as expressed by the characteristic velocity efficiency was based on vacuum specific impulse obtained from thrust and propellant flow measurements. The sequence of equations used was as follows:

$$F_{vac} = F_m + P_o A_{ex} \tag{1}$$

where F_{vac} is the vacuum thrust, F_m is the measured thrust, P_o is the ambient pressure, and A_{ex} is the area at the nozzle-exit plane.

$$I_{vac} = \frac{F_{vac}}{\dot{W}} \tag{2}$$

where I_{vac} is the vacuum impulse, $\dot{W}$ is the total propellant weight flow

$$\eta I_{vac} = \frac{I_{vac,\,exp}}{I_{vac,\,th\,eq}} \tag{3}$$

where ηI_{vac} is the vacuum impulse efficiency, subscript exp is experimental, and subscript th eq is theoretical shifting equilibrium

$$\eta C^* = \frac{\eta I_{vac}}{\eta C_{F_{vac}}} = \frac{\eta I_{vac}}{0.983} \tag{4}$$

where ηC^* is characteristic velocity efficiency and 0.983 is the calculated nozzle-thrust-coefficient efficiency (ref. 3).

Characteristic velocity-efficiency calculations were also made based on injector-end chamber pressure and propellant-flow measurements with the equation:

$$C^* = \frac{0.941\ P_c g A_T C_D}{\dot{W}}$$

In this equation, C^* is characteristic velocity, P_c is the measured injector end pressure, $\dot{W}$ is the total propellant-flow rate, A_T is the nozzle-throat area, g is the gravitational constant, and C_D is the nozzle-discharge coefficient (0.994). The factor 0.941 accounts for the momentum pressure loss when applied to the injector end measurement. This correction factor of 0.941 was obtained by a total-pressure probe inserted into the exit end of the heat-sink nozzle and located on the nozzle centerline at the throat plane. The probes were cooled by encasing the steel tubes in an ablative plastic which made possible run durations of 5 to 7 seconds.

The combustion performance was evaluated periodically to check for possible injec-

tor deterioration by substituting a heat-sink nozzle for the ablative-material section and conducting short-duration firings over an oxidant- to fuel-ratio range of 1.6 to 2.2.

A C* efficiency of 0.970±0.003 was obtained from thrust and also from the corrected chamber pressure during the heat-sink runs. The value calculated for all ablative runs, obtained from thrust after the initial 5 seconds into each run, was 0.970±0.005. A detailed description of these calculations is included in reference 3.

Three methods were used to determine the radius change of the ablative nozzle as a function of run time: (1) average throat-diameter measurements by a micrometer before and after each run, (2) throat photography followed by enlargement for subsequent integration of area and conversion to an equivalent throat-radius change, (3) propellant-flow rates. The throat radius change is related to the change in the total propellant-flow rate by the equation defining C* which uses the experimental characteristic exhaust velocity (ft/sec) (m/sec) calculated from thrust measurements on the heat-sink engines, the measured injector end chamber pressure, and the propellant flow. Solving this equation for throat radius R_T at any time during the run gives

$$\Delta R_T = \left[\left(\sqrt{\frac{C^*\dot{W}}{\pi g C_d P_c\, 0.941}}\right) - R_{To}\right]\times 10^3$$

which is the radius change. The symbol R_{To} refers to the initial throat radius at time zero. The precision of the radius change calculation was estimated to be ±0.008 inch (±8 mils (0.203 mm)) at a 95-percent confidence level. Figure 8 shows a typical curve; figure 9 shows the correlation of the three methods. Although all three methods gave comparable results, the propellant-flow method was programmed into the computer to facilitate data reduction, to minimize human error, and to standardize the method of ablative-material evaluation.

RESULTS AND DISCUSSION

Characteristic Velocity Efficiency

The variation of erosion rate with small changes in injector performance is very significant, and, therefore, it was essential to maintain constant characteristic velocity efficiency throughout the program. Of equal importance was the relatively high value obtained (0.970) as it is possible not to experience dimensional ablation if the injector efficiency is too low. Checks on the characteristic velocity efficiency were made using the heat-sink nozzle after every second or third ablative-material nozzle run. The characteristic velocity efficiency calculated from thrust measurements was maintained at 0.970 throughout the entire test program, indicating no deterioration of the injector.

When the throat radius change was plotted against run time, a typical curve corresponding to the one produced in figure 8 was obtained. The typical nozzle erosion curve can be divided into three major portions. The first section of the curve, the area under the zero erosion line, is defined as "reduced effective throat area." This decrease in the effective throat area is caused by resin decomposition and subsequent discharge of the pyrolysis products into the boundary layer together with material swelling and expansion effects which occur throughout the entire firing but are particularly pronounced during the initial firing phase. The type and percent of resin, reinforcement, and modification agents have an appreciable effect on the magnitude and duration of the curve under the zero erosion line. These variables are discussed in some detail as functions of individual nozzle firings. The second section of the curve represents steady-state erosion, and the last section shows accelerated erosion near the end of the run, indicating complete char to the insulation (resin depletion) and/or fiber deterioration which results in rapid char-layer removal.

In an effort to gain an understanding of the cause-effect relation of the various material and processing techniques involved, individual nozzles were compared to each other with respect to a major variable and are discussed in the following sections. Although only one nozzle of each type was tested and the statistical confidence level is not high, the discussion is meant to serve as a possible guide to future studies.

Fabric-fiber diameter. - Nozzles 5 and 8, presented in figure 9, compare the erosion resistance of two basic fabric weaves. Nozzle 5 was made from a high-silica cloth in which the individual fiber strands or filament bundles are approximately one-half the diameter (0.008 in. (0.203 mm) compared with 0.015 in. (0.381 mm)) of the fiber strands used to fabricate nozzle 8. The erosion resistance of the smaller-diameter fiber material was slightly superior to the larger-diameter fiber material, especially near the end of the firing.

The superior erosion resistance of the smaller-diameter fiber over the larger-diameter fiber possibly may be explained in terms of fiber surface area. The smaller individual fiber diameters will result in a nozzle in which the reinforcement has a larger total surface area. The increased surface area promotes easier penetration of the individual fibers by the impregnating resin, which in turn effects the homogeneity and tends to increase the density of the resultant char and to improve the shear force resistance.

Silica fabric and material of 1/2-inch chopped squares. - Nozzles 10 and 11, presented in figure 10, are a comparison of the erosion resistance between a silica-powder-filled phenolic system employing a fabric layup 90° to centerline and a chopped molding compound of 1/2-inch squares randomly orientated. Nozzle 10, the fabric layup, appeared to be slightly superior to the chopped molding compound, nozzle 11.

The relatively short fiber length associated with the material of 1/2-inch squares apparently has a degrading effect on the nozzle tensile strength and shear force resistance of the resulting char. It appears to be advantageous to have the individual fibers firmly anchored within a portion of the virgin material for as long a period of time during the run as possible.

Rosette layup with and without additives. - Nozzles 1, 2, 3, and 4 were tested to compare the relative erosion resistance of a rosette-type layup. Erosion data for all four nozzles are presented in figure 11.

Nozzle 1 contained a chromium salt, which was added to the large-diameter cloth material prior to impregnation. The overall erosion rate, after 250 seconds run time, was calculated at 1.280 mils per second (0.0325 mm/sec).

Nozzle 2 again contained the chromium-salt additive to the large-diameter cloth, but, in this case, the coated cloth material was subjected to an additional proprietary process which converted the cloth-salt combination to a more refractory-type reinforcement. An improvement in the overall erosion resistance over nozzle 1 was obtained and was calculated to be 0.930 mil per second (0.0236 mm/sec).

Since previous testing had indicated that smaller-diameter cloth might be superior in erosion resistance to larger-diameter cloth material, an attempt was made to procure a third nozzle which was identical to nozzle 2, except that the small-diameter cloth material would be used. Unfortunately, this nozzle configuration did not prove possible as the small-diameter cloth material lost approximately 80 percent of its physical strength during the proprietary conversion process. As an alternative approach, the small-diameter cloth containing the chromium-salt additive was impregnated with a new proprietary resin system in the hope that, upon firing in a rocket engine, the resultant composite would duplicate the refractoryness of nozzle 2. Since a chemical analysis was not performed on both nozzles prior to and after each firing to determine the type of refractory formed, nozzle 3 can only be evaluated on the basis of its initial constituents. A relatively high erosion rate of 1.280 mils per second (0.0325 mm/sec) would indicate no particular advantage from this alternate material. The potential advantages of the chromium-salt conversion process (as shown by the comparative erosion rates of nozzles 1 and 2) may prove promising, expecially if a method is found to treat the small diameter cloth, although careful attention to processing variables would be required.

Nozzle 4 was made from small-diameter cloth and contained no chromium-salt additive. The overall erosion rate was the lowest of any material tested in the program, 0.640 mil per second (0.01625 mm/sec). This superior performance may have been due to the small-diameter fiber, absence of chromium-salt additive, rosette helix angle, or some combination of all three. The inability to treat the chomium-salt material without destroying the strength of the small-diameter fibers was unfortunate.

Figure 12 shows all four nozzles after firing. After sectioning of the nozzles, it was

discovered that the helix angle of layup varied and was approximately 5° for nozzle 1, 20° for nozzles 2 and 3, and approximately 35° for nozzle 4. Since other variations were involved, a meaningful assessment of the effect of helix angle on erosion rate was not possible.

Unidirectional and two-dimensional cloth weaves. - The advantage, if any, of orienting all the fiber strands in a single direction perpendicular to the gas flow was determined by modifying a standard two-dimensional light-weight cloth material by removing all the fill fiber strands and leaving warp (radial) strands only. The resin content and final density remained constant. Figure 13 compares the erosion resistance of the unidirectional fibers (nozzle 6) with a standard two-dimensional weave (nozzle 5).

The superior erosion resistance of the unidirectional fibers might be attributed to (1) the increase in the actual number of fibers exposed directly to the gas stream, thereby increasing the nozzle shear resistance and (2) the relative ease by which the decomposed resin gases may permeate through to the surface and enter the boundary layer during the early portion of the run.

An orientation of 90° to the nozzle centerline of the unidirectional material results in a high thermal conductivity of the composite and also affords a direct path for the gases to escape. Since it is desirable to maximize the heat absorbed by endothermic reactions (formation of refractory SiC, graphites, etc.) between the gases and the reinforcing matrix, the dwell time of the gases becomes an important parameter. Increasing the dwell time and hopefully absorbing more energy could be accomplished by reducing the orientation angle of the unidirectional material from 90° to some lower value. A possible further increase in the overall erosion resistance of nozzle 6 may be expected. This procedure would be particularly applicable to long firing durations.

High and low resin content. - The unidirectional fabric was chosen to assess the gross effect of resin concentration on erosion rate. Figure 14 compares the erosion resistance of a 22-percent resin content material (nozzle 6) to a material containing 35-percent resin (nozzle 7). Although nozzle 7 experienced the same effective radius change for the first 100 seconds, nozzle 6 was superior for the remainder of the run and had a greater overall resistance to erosion.

The excess resin of nozzle 7 compared to nozzle 6 provided additional cooling capacity during the early portion of the run. For longer firing durations, however, the reduced reinforcement content proved detrimental. The magnitude and duration of both curves under the zero erosion line indicates the relative ease by which the decomposed resin gases are able to enter the boundary layer for the unidirectional fibers.

Best and Least Erosion-Resistant Materials Studied

Nozzle 4 represents the accumulative effect on the erosion resistance when many of the variables, previously explored individually, are incorporated into one nozzle. The results may be considered an approach to optimization. Nozzle 4, which had the greatest resistance to erosion, is plotted on figure 15 together with the data for nozzle 9, which demonstrated the least resistance to erosion.

The extended time (117 sec) for nozzle 4 to experience positive erosion is caused primarily by the evolution of decomposition products of the resin binder into the boundary layer. The relatively rapid initiation of positive erosion for nozzle 9 was due to the very low percentage of resin binder (13 percent). In addition, the silicone resin copolymer results in a very small percentage of gaseous decomposition products available for cooling purposes. During steady state operating, the small-diameter cloth, high char density, and rosette layup all contributed to the greater erosion resistance of nozzle 4, while the lower erosion resistance of nozzle 9 was apparently a function of the low shear force resistance of the elastomeric additive (25 percent).

A significant effect on the erosion rate may also be seen in figure 15. After 140 seconds of normal running on nozzle 9, the injector became unstable. The rapid increase in the erosion rate for the last 10 seconds of operation was quite pronounced. The frequency of the instability was measured at 2200 cycles per second (2200 Hz). A subsequent (stable) run on nozzle 9, from 150 to 250 seconds, made with the same injector, resulted in an erosion rate equivalent to the first run prior to the instability.

Comparison of All Nozzles Tested

A summary of the test results is presented in table II, which lists the ablative nozzles in order of decreasing erosion resistance. One nozzle (4) was run for 325 seconds, four nozzles (5, 7, 8, and 10) were run for 350 seconds, and the six remaining nozzles were run for 250 seconds. For direct comparison, the overall erosion rates (change in radius/run time) were calculated for the initial 250 seconds. Data concerning char are also included and are presented as the percent char to the asbestos insulation, as a function of the original wall thickness, after the firing has been completed. Char was measured at the throat plane only since some gouging did occur, and the char formation is meant to be an estimate for comparison only.

Typical chars are presented in figures 16 and 17. Nozzle 4 had less than one-half the erosion rate after 250 seconds of firing that nozzle 9 exhibited. However, both experienced the same percent char, although nozzle 4 was run 75 seconds longer. For a

constant erosion rate, a low char rate would require less insulation; thereby, a weight saving would be effected. The rosette layup appeared to decrease the char rate while it maintained a low erosion rate.

CONCLUDING REMARKS

The results from the investigation strongly suggest that it is possible to optimize an ablative composite to meet the requirements of a range of storable-propellant rocket-engine duty cycles. Ablatives for short-duration firings could be tailored to maximize the area under the zero erosion line. This increase may be accomplished by controlling the volume and chemical species injected into the boundary layer. As firing durations became longer, the properties of the reinforcement such as fiber strength, viscosity, and melting temperature became more important.

New resin systems are presently being developed under contract NAS3-7949 to improve the heat absorption characteristics and char formation properties when used with high-silica or other refractory reinforcements. New type fibers being developed under contract NAS3-7948 may extend the useful temperature range of ablative composites significantly above the present level.

Until such time as these potential improvements prove practical, however, much can be done within the present state of the art.

SUMMARY OF RESULTS

An investigation was conducted to evaluate 11 high-purity-silica reinforced ablative-material samples as nozzle sections of a storable propellant nitrogen-tetroxide (N_2O_4 and a 50-50 blend of unsymmetrical dimethylhydrazine UDMH with hydrazine N_2H_4) rocket engine. Testing was performed at an oxidant-to-fuel ratio of 2.0, a chamber pressure of 100 psia (689 kN/m^2), and a nominal throat diameter of 7.82 inches (19.8 cm).

1. Lightweight (small fiber diameter) high-purity-silica cloth had slightly higher erosion resistance than heavyweight high-purity-silica cloth.

2. Heavyweight high-purity-silica cloth, with fibers oriented 90° to the nozzle centerline, had slightly higher erosion resistance than heavyweight high-purity-silica cloth of molded 1/2-inch squares.

3. A modified (proprietary treatment) chromium-salt additive to a heavyweight silica cloth was more erosion resistant than an unmodified chromium-salt additive to a heavyweight high-purity-silica cloth when both are layed up in a rosette pattern.

4. A unidirectional-type fiber orientation was more erosion resistant than a standard two-dimensional-type weave.

5. A unidirectional lightweight high-purity-silica material impregnated with 22-percent polyamide phenolic resin was more erosion resistant than the same material impregnated with 35-percent polyamide phenolic resin.

6. The most erosion-resistant material of those tested was a lightweight high-purity-silica cloth material impregnated with 27-percent polyamide phenolic resin, layed up in a 35° rosette pattern with no additive to the cloth material.

7. The least erosion-resistant material tested was a heavyweight high-purity-silica cloth impregnated with 25-percent elastomer and 13-percent phenylsilane resin with fibers oriented 90° to the nozzle centerline.

Lewis Research Center,
National Aeronautics and Space Administration,
Cleveland, Ohio, March 13, 1967,
128-31-03-01-22.

REFERENCES

1. Salmi, Reino J.; Wong, Alfred; and Rollbuhler, Ralph J.: Experimental Evaluation of Various Nonmetallic Ablative Materials as Nozzle Sections of Hydrogen-Oxygen Rocket Engine. NASA TN D-3258, 1966.

2. Peterson, Donald A.; and Meyer, Carl L.: Experimental Evaluation of Several Ablative Materials as Nozzle Sections of a Storable-Propellant Rocket Engine. NASA TM X-1223, 1966.

3. Shinn, Arthur: Experimental Evaluation of Six Ablative Material Thrust Chambers as Components of Storable Propellant Rocket Engines. NASA TN D-3945, 1967.

TABLE I. - ABLATIVE-MATERIAL SAMPLES

Nozzle	High-silica reinforcement						Binder				Molding conditions				
	Cloth			Additive		Orientation	Resin		Additive		Temperature		Pressure		Time, hr
	Fiber diameter		Weight, percent	Type	Weight, percent		Type	Weight, percent	Type	Weight, percent	°F	°C	psia	kN/m^2	
	in.	mm													
1	0.015	0.381	71	Chromium salts	2	Rosette, 5°	Phenolic	27	Polyamide	--	350	177	1000	6 895	4
2	.015	.381	71	Chromium salt, proprietary modification	2	Rosette, 20°			Polyamide	--					
3	.008	.203	71	Chromium salts	2	Rosette, 20°			Proprietary modification	--					
4	.008		73	None	--	Rosette, 35°			Polyamide	--					
5	.008		77		--	90°		23		--	325	163	3000	20 685	3
6	.008 (unidirectional)		78					22		--					
7	.008 (unidirectional)		65					35		--					
8	.015	.381	80		--			20		--					
9			62		--		Phenyl silane	13	Elastomer	25					
10					--		Phenolic	30	Fine silica powder	8					
11						1/2-inch squares	Phenolic	30	Fine silica powder	8					

TABLE II. - TEST RESULTS

Nozzle	Throat diameter				Erosion rate after 250-sec run		Area change after 250-sec run, percent	Char to insulation		Condition of throat after firing	Nozzle description
	Initial		After 250-sec run		mil/sec	cm/sec		Percent	After run of - sec		
	in.	cm	in.	cm							
4	7.818	19.83	8.137	20.67	0.6383	1.622	8.34	62	325	Minor gouging, moderate delamination, spallation in char	Small diameter, cloth rosette
6	7.831	19.89	8.280	21.02	.932	2.368	12.25	---	---	----------	Small diameter, unidirectional low resin
2	7.828	19.87	8.2936	21.03	.93415	2.372	12.25	60	250	Minor gouging, moderate delamination, spallation in char	Large diameter, modified rosette
10	7.8298	19.88	8.4040	21.35	1.060	2.690	13.99	100	350	Minor gouging, char to outside diameter, slight delaminations	Large diameter, fine silica powder filled
5	7.829	19.88	8.403	21.35	1.150	2.920	15.22	---	---	----------	Small diameter, 90^{o} layup
7	7.811	19.80	8.384	21.30	1.150	2.920	15.22	65	350	Minor gouging, moderate cracking and delaminations	Small diameter, unidirectional high resin
11	7.8295	19.88	8.407	21.35	1.158	2.940	15.33	70	250	Minor gouging, minor cracks in char	Large diameter, 1/2-inch squares, fine silica powder
8	7.823	19.85	8.4248	21.40	1.205	3.055	15.98	100	350	Minor gouging, char to outside diameter, severe delaminations	Large diameter, 90^{o} layup
1	7.826	19.86	8.462	21.47	1.273	3.235	16.93	60	250	Minor gouging, moderate delamination, spallation in char	Large diameter, rosette
3	7.825	19.86	8.4819	21.55	1.274	3.238	17.50	60	250	Minor gouging, moderate delamination, spallation in char	Small diameter, rosette, modified resin
9	7.822	19.85	8.632	21.92	1.635	4.155	21.85	62	250	Minor gouging, minor delamination	Large diameter, elastomeric phenyl silane

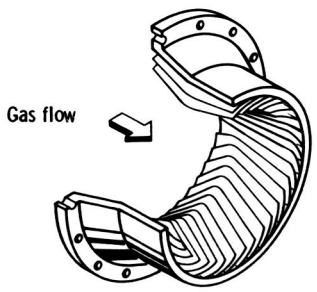

(a) Rosette.

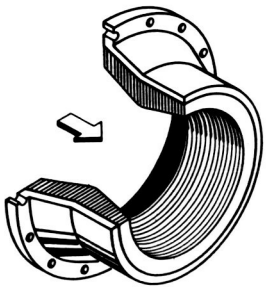

(b) Fiber-orientation angle, 90°.

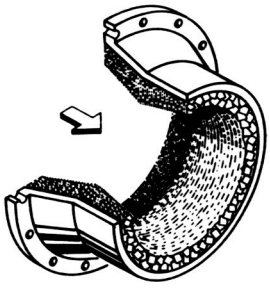

CD-9005

(c) Material of 1/2-inch chopped squares.

Figure 1. - Nozzle configurations.

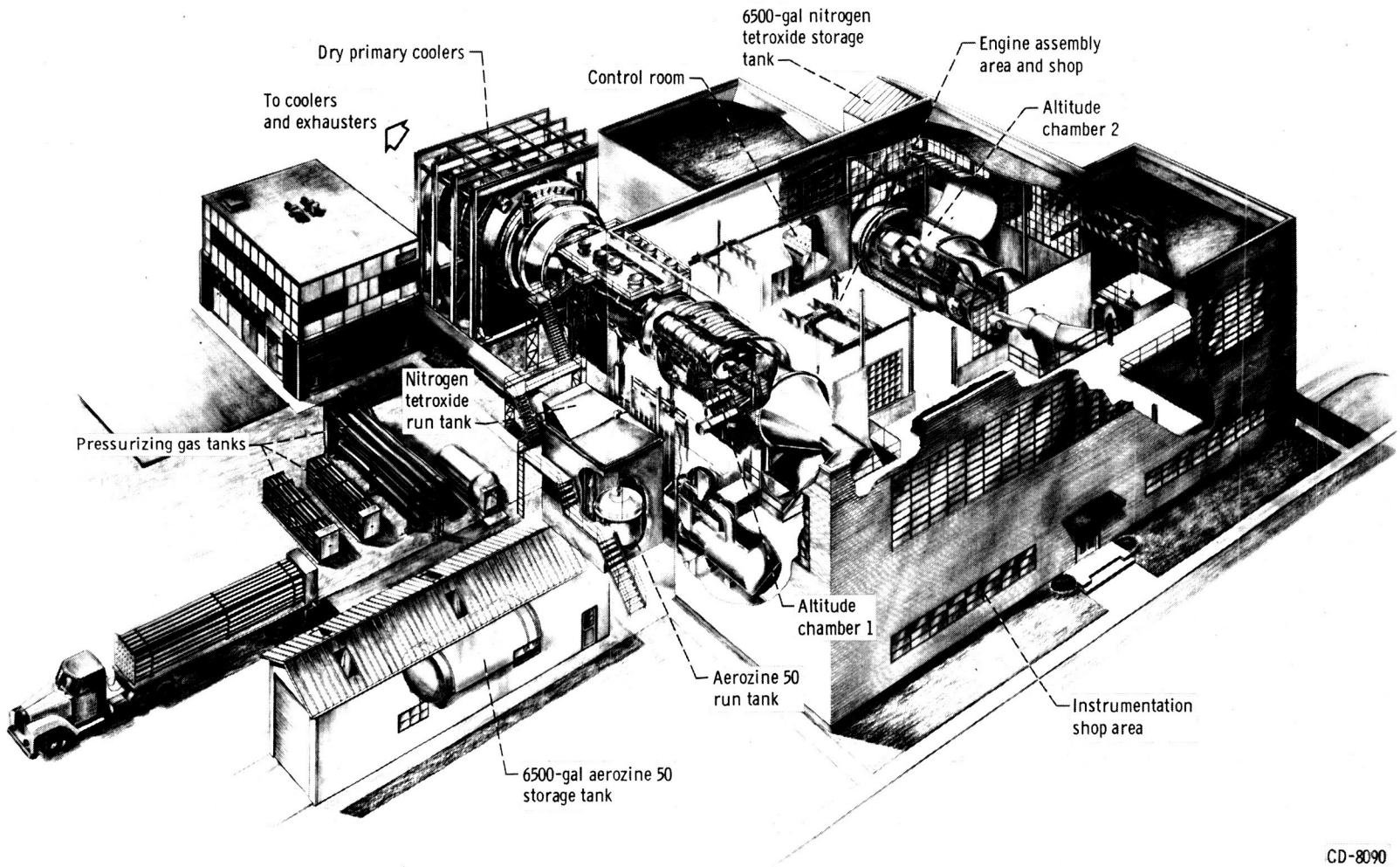

Figure 2. - Altitude facility.

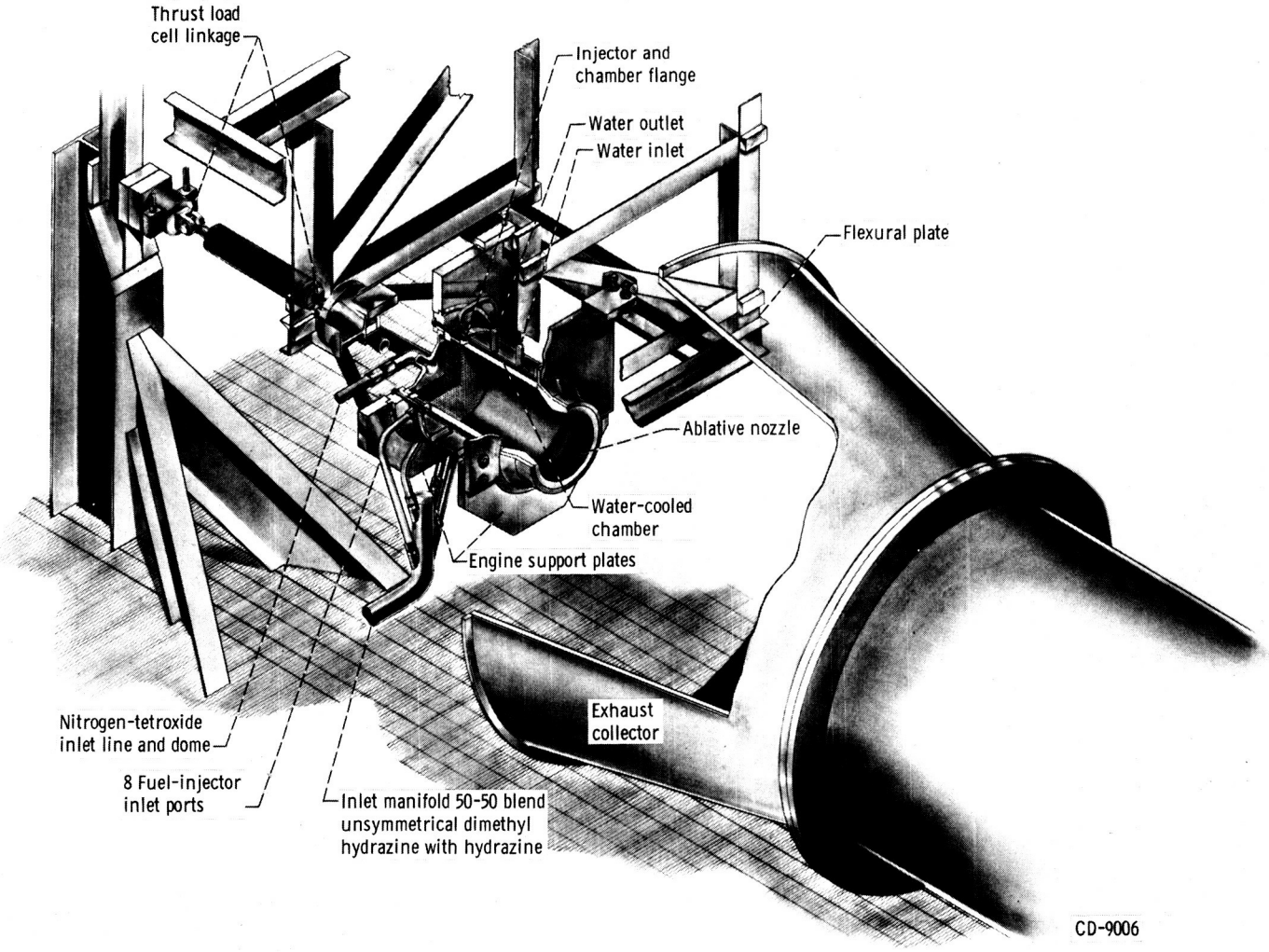

Figure 3. - Cutaway view of test chamber and injector assembly.

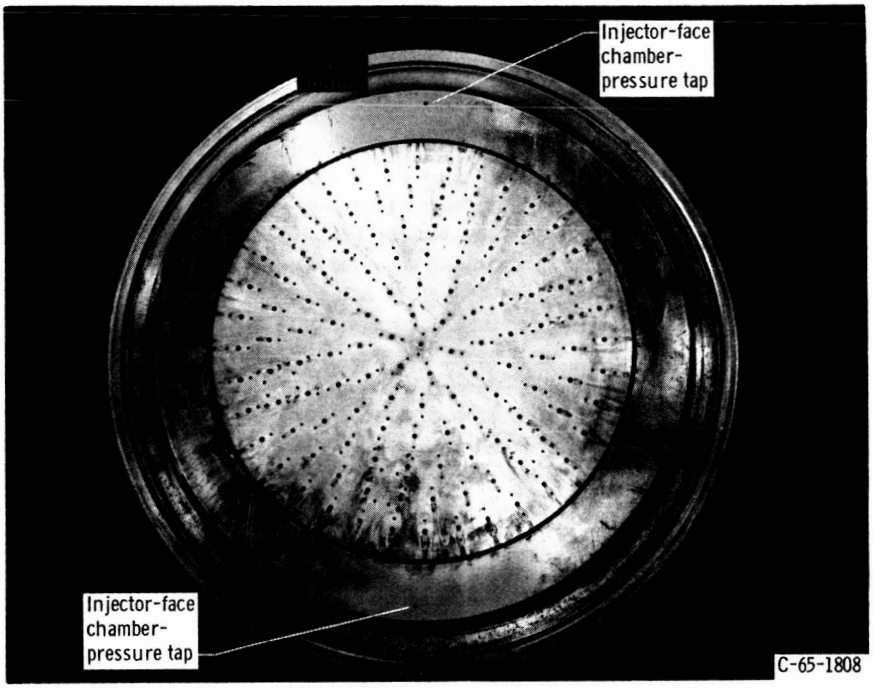

Figure 4. - Injector.

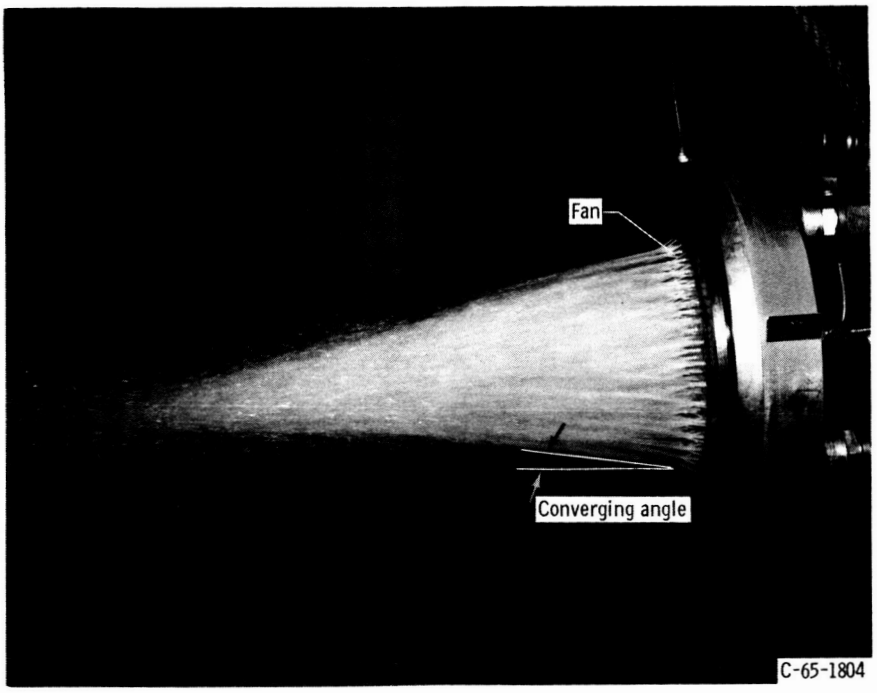

Figure 5. - Water-flow test.

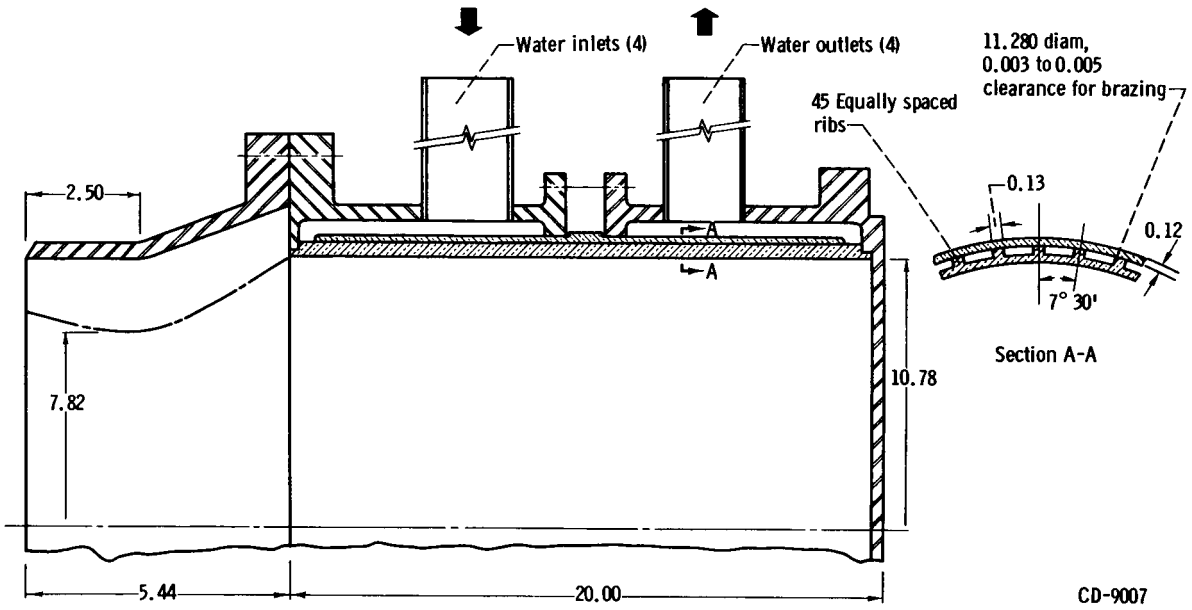

Figure 6. - Water-cooled combustion chamber and nozzle assembly. All linear dimensions are in inches. Multiply by 2.54 to convert to centimeters.

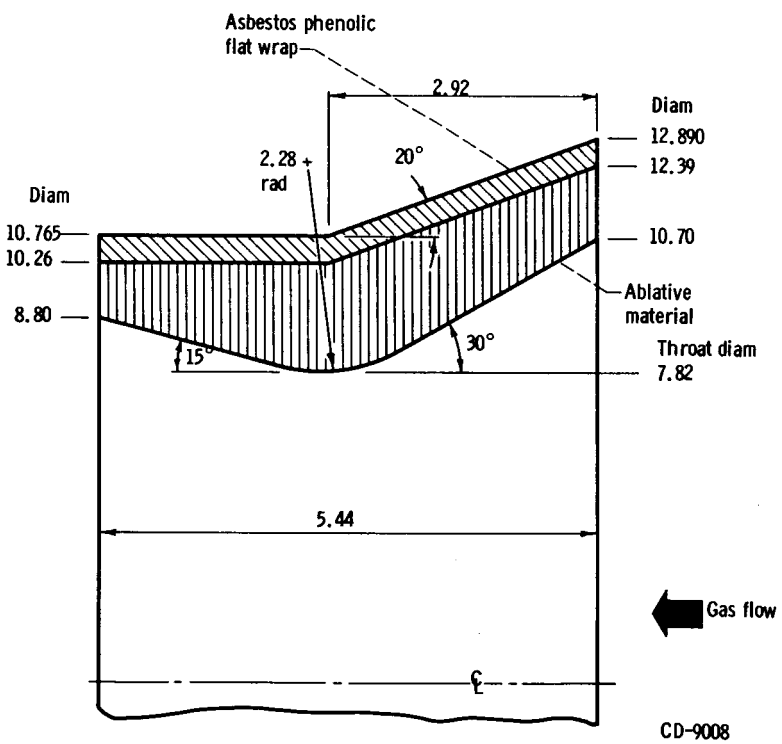

Figure 7. - Ablative nozzle. All linear dimensions are in inches. Multiply by 2.54 to convert to centimeters.

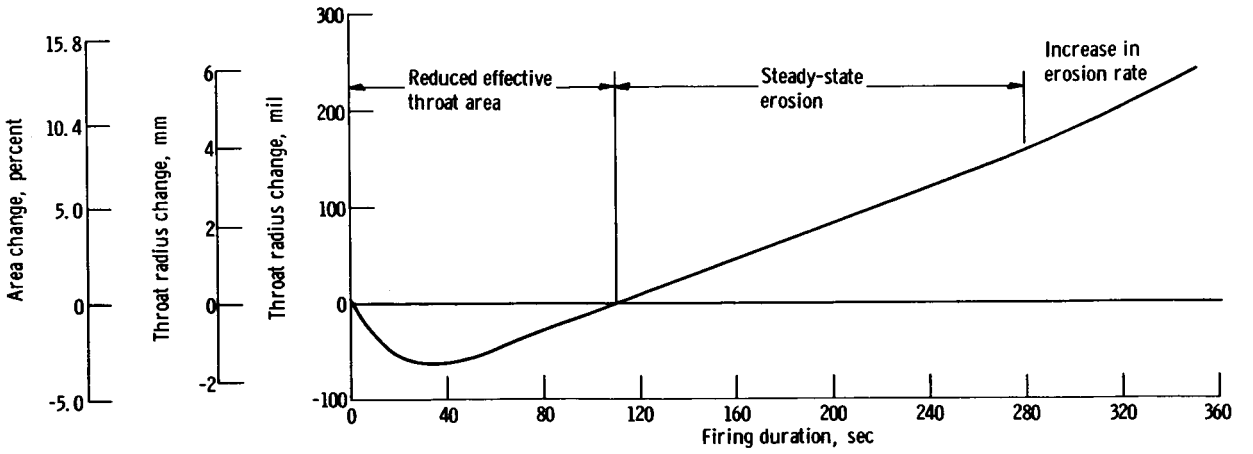

Figure 8. - Typical nozzle erosion curve.

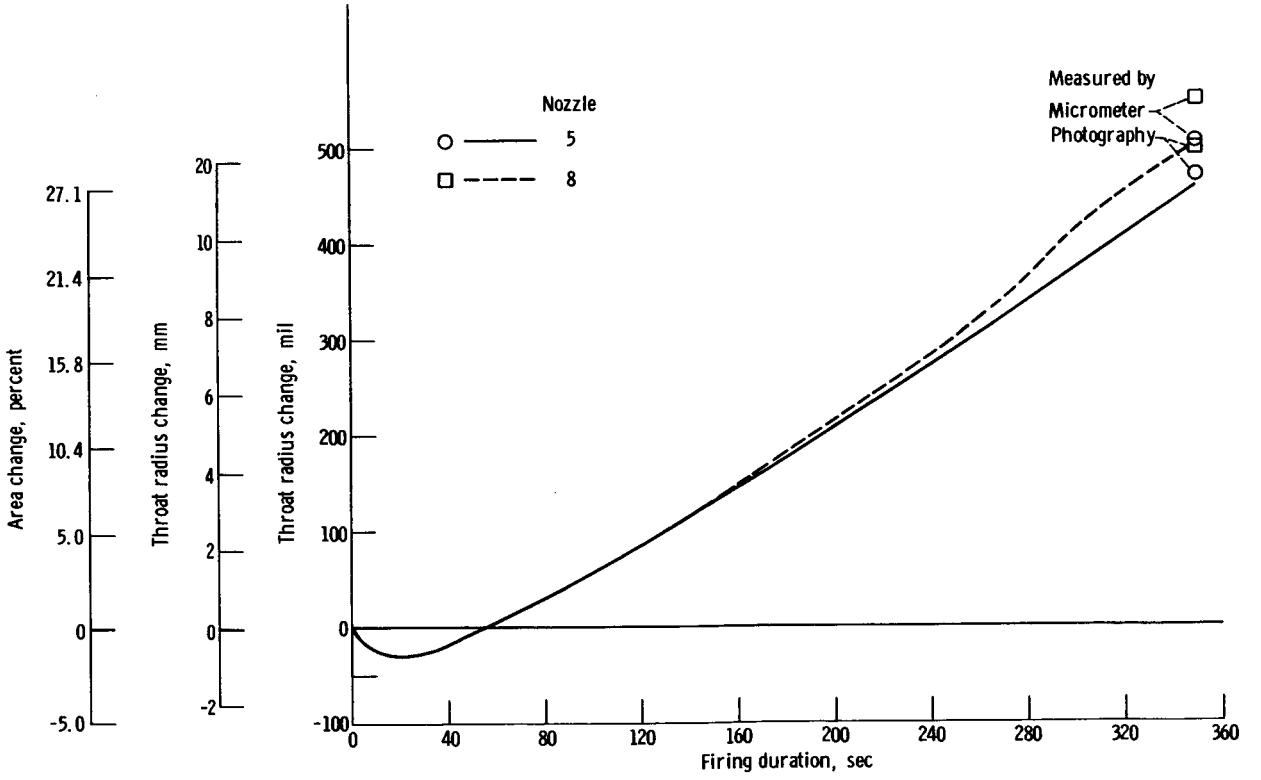

Figure 9. - Erosion for nozzle 5, small-diameter fiber, 90° fiber-orientation angle, and nozzle 8; large-diameter fiber, 90° fiber-orientation angle.

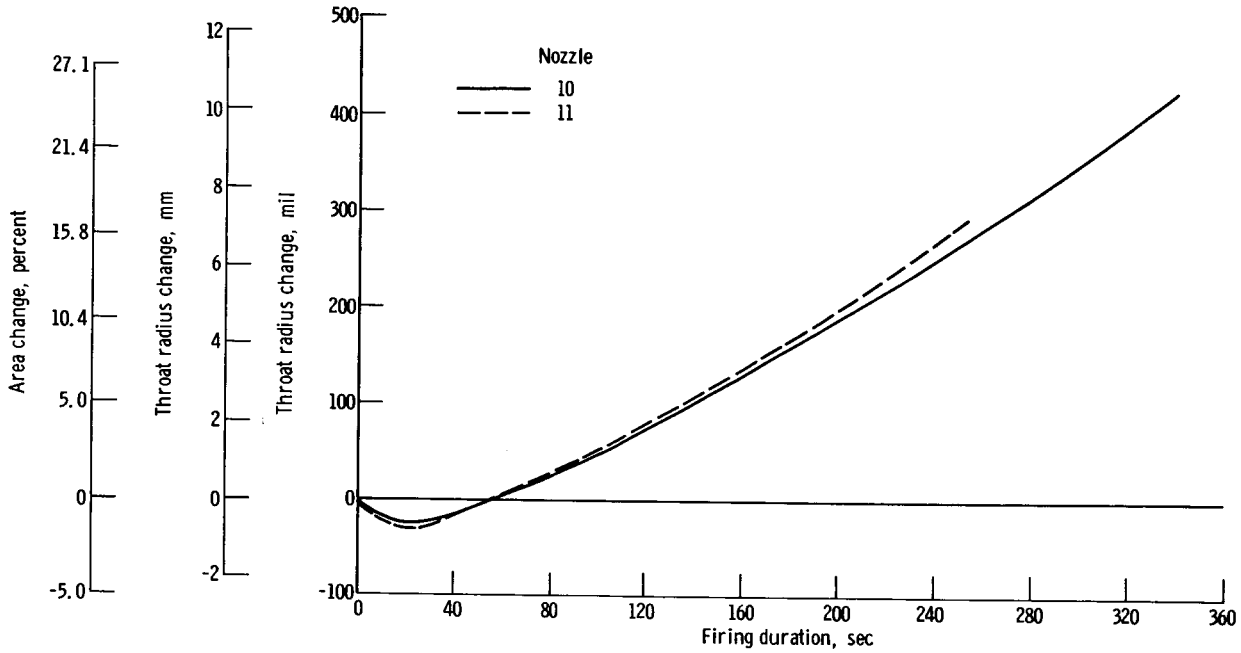

Figure 10. - Erosion for nozzle 10, fabric material, 90° fiber-orientation angle, and nozzle 11, material of 1/2-inch chopped squares.

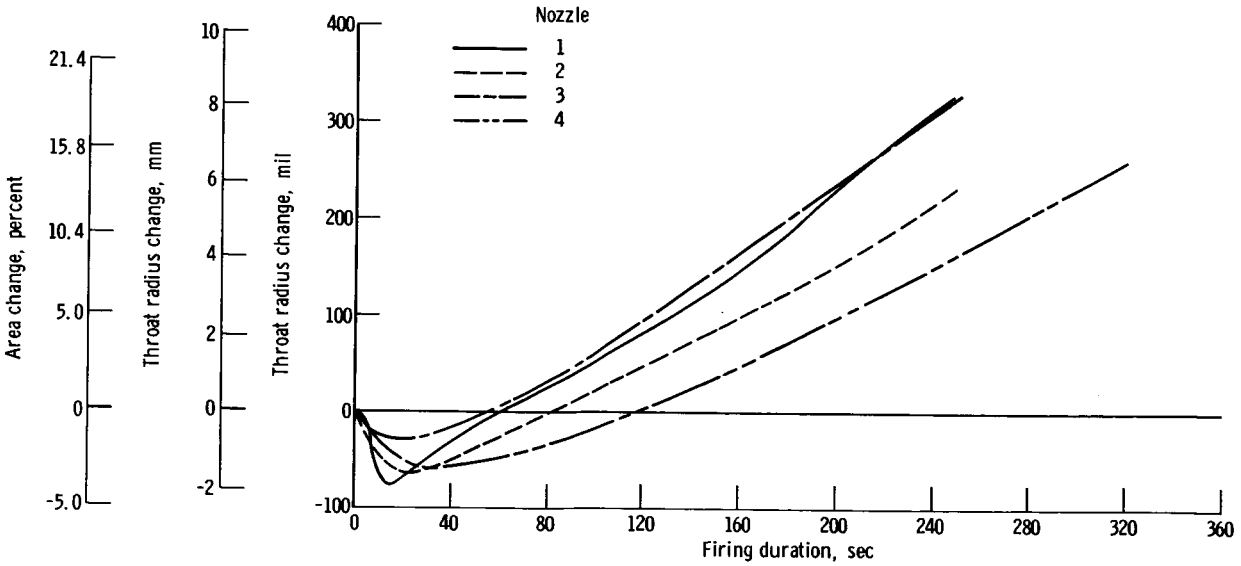

Figure 11. - Rosette layup for nozzle 1, large-diameter fiber, green cloth; nozzle 2, large-diameter fiber, modified green cloth; nozzle 3, small-diameter fiber, green cloth, resin modified; and nozzle 4, small-diameter fiber cloth.

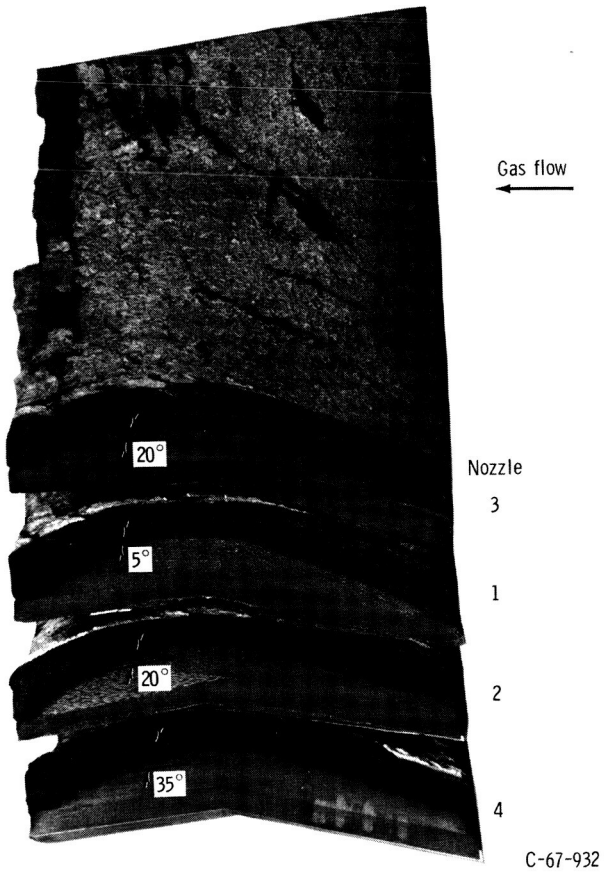

Figure 12. - Postfiring examination showing rosette layup angle of orientation.

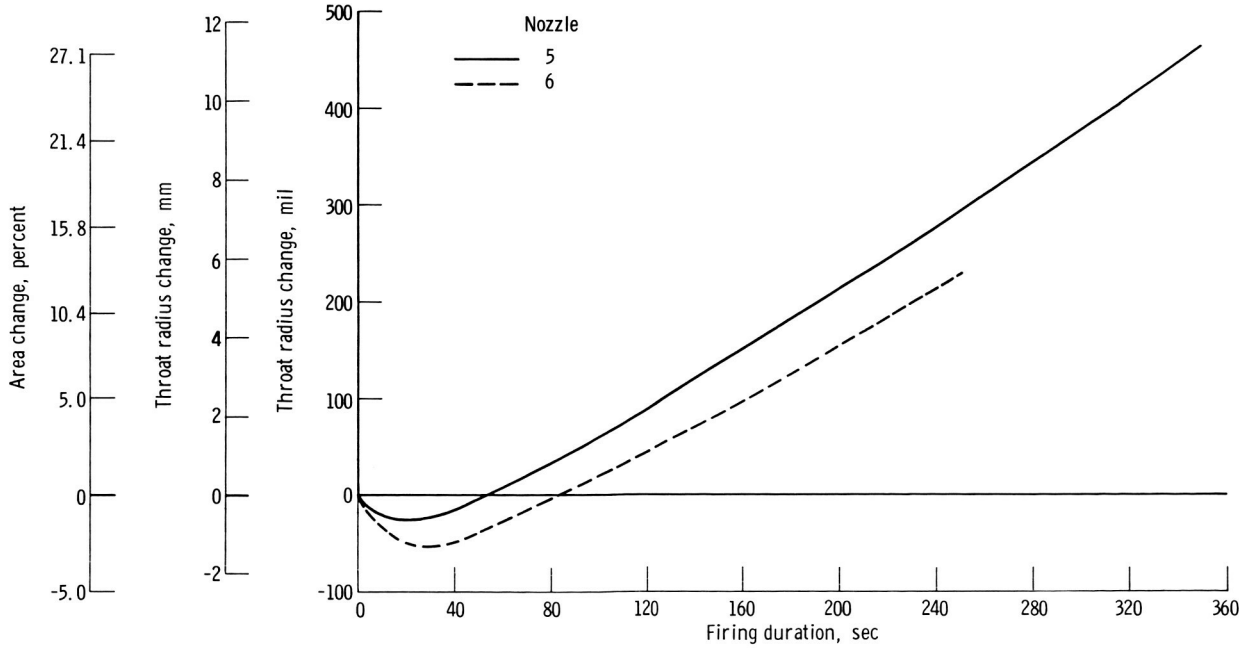

Figure 13. - Erosion for nozzle 5, small-diameter fiber, two-dimensional-weave cloth, 90° fiber-orientation angle, and nozzle 6, small-diameter, unidirectional-fiber cloth.

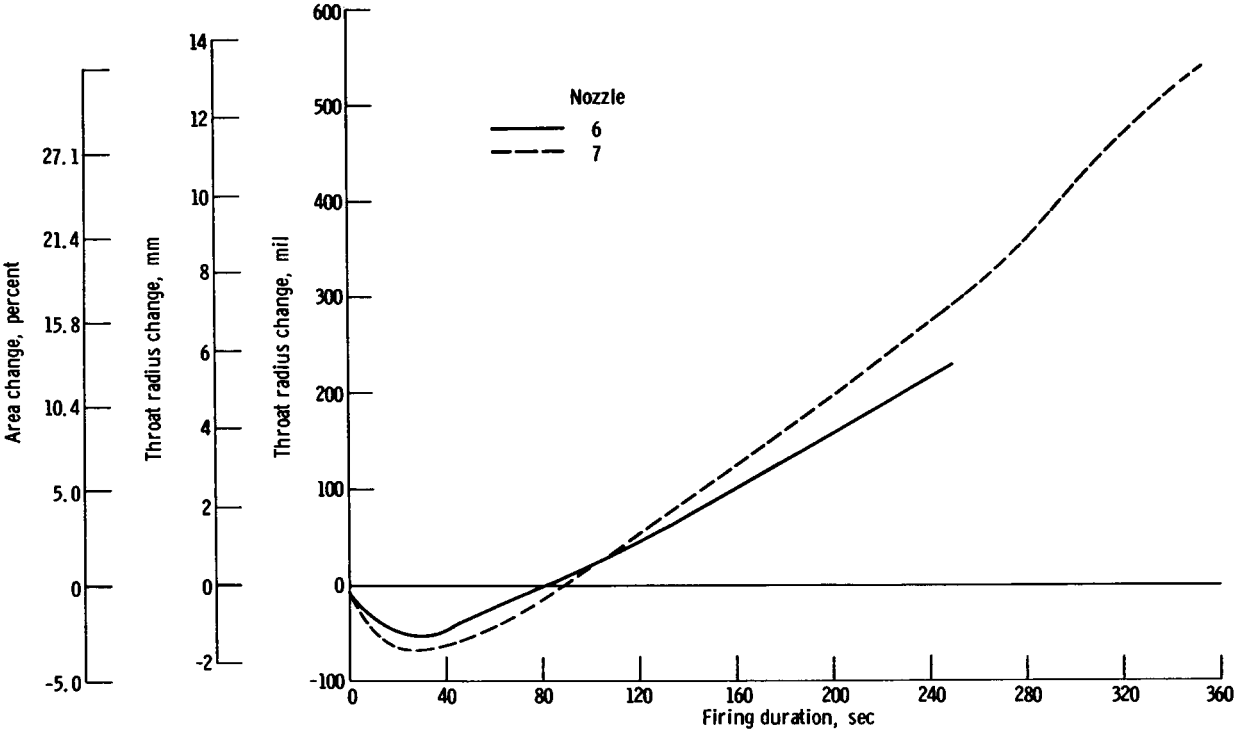

Figure 14. - Erosion for nozzle 6, low resin content (22 percent) and nozzle 7, high resin content (35 percent).

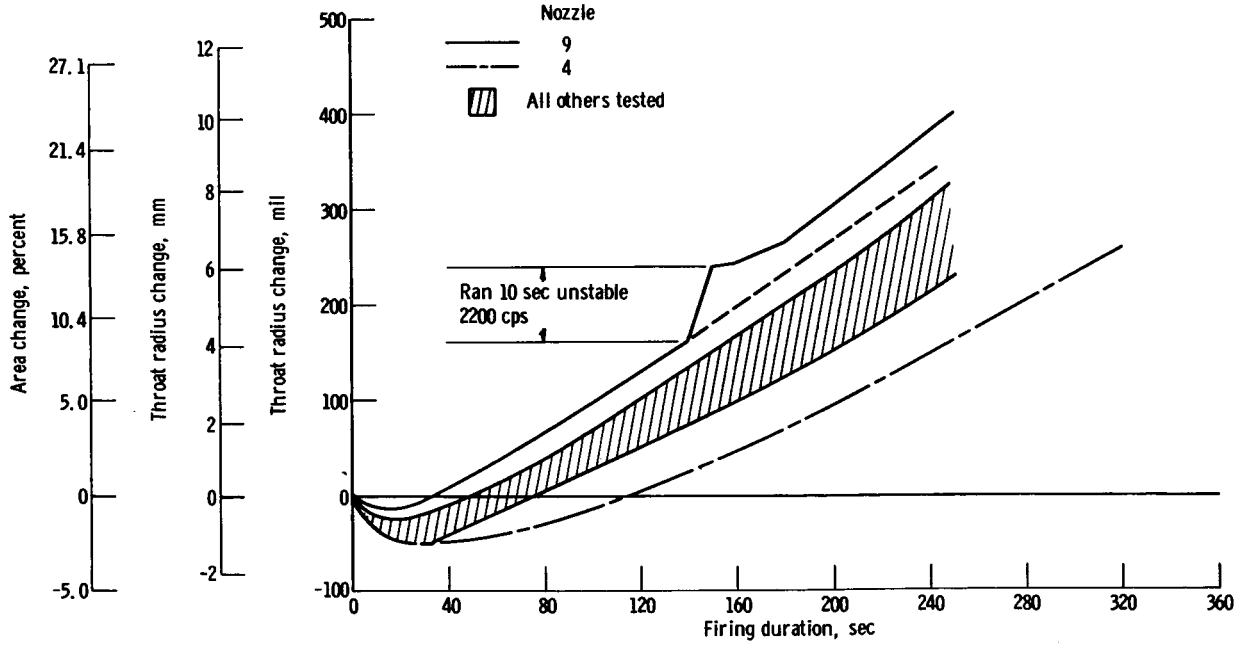

Figure 15. - Comparison of erosion of nozzle 9, heavyweight elastomer filled; nozzle 4, lightweight rosette; and all other nozzles tested.

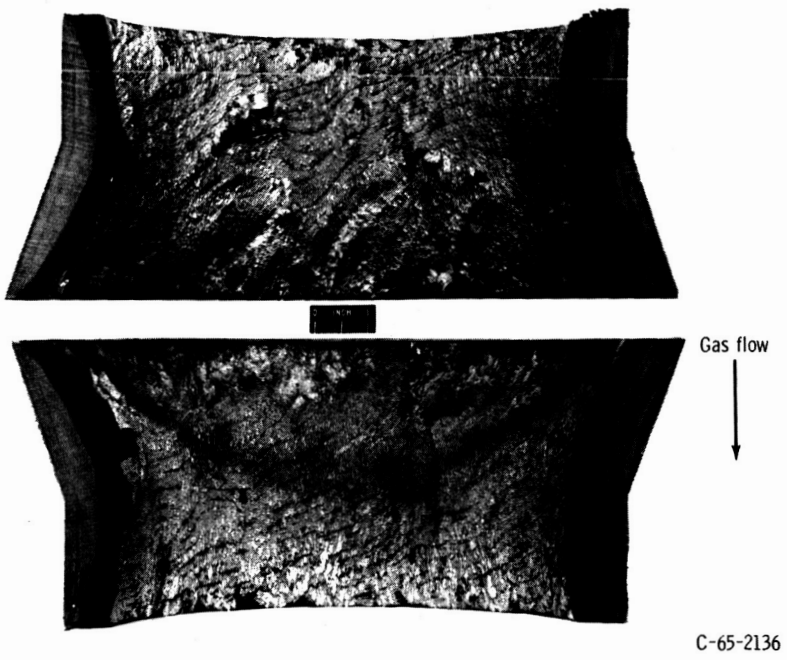

Figure 16. - Char formation, nozzle 4.

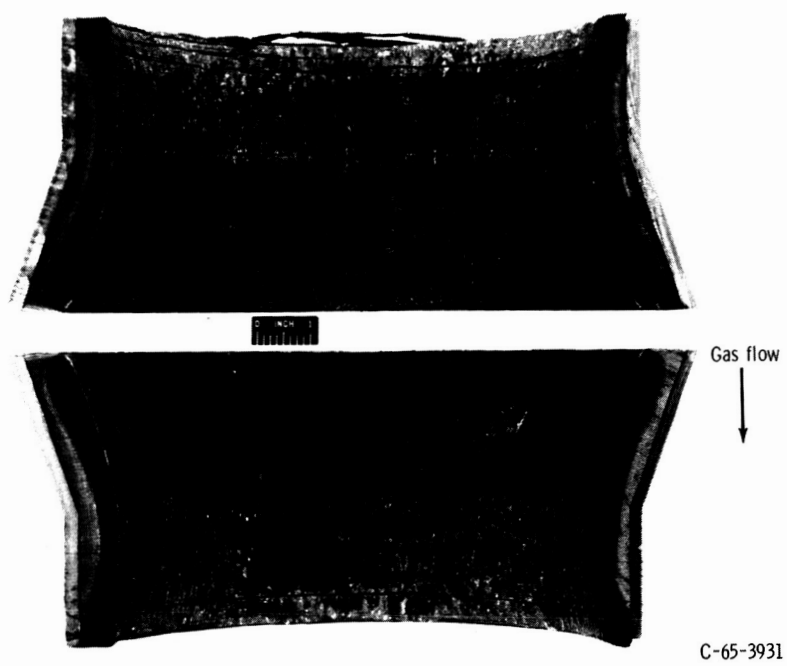

Figure 17. - Char formation, nozzle 9.